JACS
JOURNAL OF THE AMERICAN CHEMICAL SOCIETY
Article
pubs.acs.org/JACS

Introduction of π-Complexation into Porous Aromatic Framework for Highly Selective Adsorption of Ethylene over Ethane

Baiyan Li,[†] Yiming Zhang,[†] Rajamani Krishna,[‡] Kexin Yao,[§] Yu Han,[§] Zili Wu,[∥] Dingxuan Ma,[⊥] Zhan Shi,[⊥] Tony Pham,[†] Brian Space,[†] Jian Liu,[#] Praveen K. Thallapally,[#] Jun Liu,[#] Matthew Chrzanowski,[†] and Shengqian Ma*[,†]

[†]Department of Chemistry, University of South Florida, 4202 E. Fowler Avenue, Tampa, Florida 33620, United States

[‡]Van't Hoff Institute for Molecular Sciences, University of Amsterdam, Science Park 904, 1098 XH Amsterdam, Netherlands

[§]Advanced Membranes and Porous Materials Center, Physical Sciences and Engineering Division, King Abdullah University of Science and Technology, Thuwal 23955-6900, Kingdom of Saudi Arabia

[∥]Center for Nanophase Material Sciences and Chemical Sciences Division, Oak Ridge National Laboratory, Oak Ridge, Tennessee 37831, United States

[⊥]State Key Laboratory of Inorganic Synthesis and Preparative Chemistry, College of Chemistry, Jilin University, Changchun 130012, People's Republic of China

[#]Pacific Northwest National Laboratory, Richland, Washington 99352, United States

Web-Enhanced Feature *Supporting Information*

ABSTRACT: In this work, we demonstrate for the first time the introduction of π-complexation into a porous aromatic framework (PAF), affording significant increase in ethylene uptake capacity, as illustrated in the context of Ag(I) ion functionalized PAF-1, PAF-1-SO_3Ag. IAST calculations using single-component-isotherm data and an equimolar ethylene/ethane ratio at 296 K reveal that PAF-1-SO_3Ag shows exceptionally high ethylene/ethane adsorption selectivity (S_{ads}: 27 to 125), far surpassing benchmark zeolite and any other MOF reported in literature. The formation of π-complexation between ethylene molecules and Ag(I) ions in PAF-1-SO_3Ag has been evidenced by the high isosteric heats of adsorption of C_2H_4 and also proved by in situ IR spectroscopy studies. Transient breakthrough experiments, supported by simulations, indicate the feasibility of PAF-1-SO_3Ag for producing 99.95%+ pure C_2H_4 in a Pressure Swing Adsorption operation. Our work herein thus suggests a new perspective to functionalizing PAFs and other types of advanced porous materials for highly selective adsorption of ethylene over ethane.

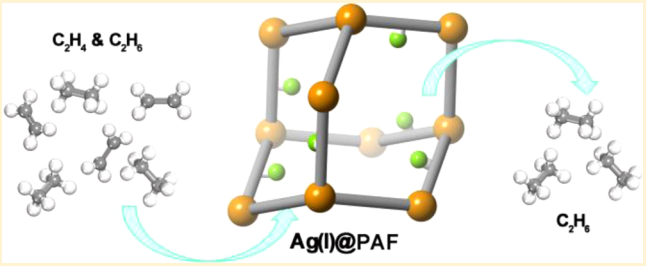

INTRODUCTION

Ethylene, one of the most widely used feedstock molecules in the petrochemical industry, is usually obtained via steam cracking and thermal decomposition of ethane.[1] The similar molecular sizes and volatilities make the separation of ethylene/ethane mixtures one of the most challenging chemical separations at large scale.[2] Current technology uses cryogenic distillation performed under the conditions of high pressure (23 bar) and low temperature (−25 °C), resulting in an extremely cost and energy intensive process.[3] Extensive efforts to develop low energy approaches for efficient ethylene/ethane separation at higher temperature and normal atmospheric pressure have focused on membrane separation,[4] organic solvent-based sorbents,[5] and porous solid adsorbents.[6] Among these approaches, porous solid adsorbents attract particular interest because of their great potential to afford much lower cost and energy consumption.

Over the past decade, advanced porous materials such as metal−organic frameworks (MOFs)[7] and porous organic polymers (POPs)[8] [e.g., porous aromatic frameworks (PAFs),[9] conjugated microporous polymers (CMPs),[10] porous polymer networks (PPNs),[11] and porous organic frameworks (POFs)[12]] have been explored as new classes of solid adsorbents for applications in gas storage,[13] gas separation,[14] carbon capture,[15] catalysis,[16] and so forth. Compared with conventional solid adsorbents of zeolites and mesoporous silica materials,[17] MOFs[7] and POPs[8] feature the amenability of design and modular nature, adjustable pore sizes, functionalizable pore surfaces, and high surface areas. These features also make them hold great promise for hydrocarbon separation,[18] including the separation of ethylene/ethane mixtures.[19]

Received: March 1, 2014
Published: June 5, 2014

dx.doi.org/10.1021/ja502119z | J. Am. Chem. Soc. 2014, 136, 8654−8660

Adsorption-based separation of ethylene/ethane using MOFs focuses on the preferential interactions between open metal sites and ethylene molecules, and high ethylene uptake capacities and ethylene/ethane selectivities have been demonstrated in MOFs with open metal sites.[19a−f]

In comparison with MOFs, POPs, despite the amorphous nature for most of them, feature robust covalent framework structures showing high water, moisture, and chemical stability;[8] they could also be readily scaled up using one-pot reactions. However, the lack of preferential binding sites for ethylene molecules leads to poor ethylene/ethane adsorption selectivity.[8c,19g] A recently reported copper(catecholate) decorated POP demonstrates enhanced ethylene/ethane selectivity;[20] nevertheless, the absolute selectivity remains low, presumably due to the moderate interactions between open Cu(II) sites and ethylene molecules. Therefore, in order to achieve high ethylene/ethane selectivity in POPs, stronger binding sites for ethylene molecules are desired.

It has been well-documented that Cu(I) and Ag(I) ions can form π-complexation with the carbon−carbon double bonds of olefin molecules in solutions,[5,6,21] and these systems have been employed for absorptive separations of olefins from paraffins, which are however inefficient because of the poor contact between the hydrocarbons and the liquid absorbents.[5] We postulate that if such kinds of π-complexation can be introduced into POP, the π-complexation will afford strong interactions between the ethylene molecules and the framework, whereas the porous structure of POP can maximize the contact of between the ethylene molecules and the framework, thereby resulting in high ethylene/ethane selectivity. In this contribution, we demonstrate for the first time the introduction of π-complexation into POPs, as illustrated in the context of functionalizing the highly porous PAF, PAF-1[22] with Ag(I) ions. The resultant PAF-1-SO_3Ag not only exhibits significant enhancement of ethylene uptake capacity compared to the parent PAF-1, but also demonstrates exceptional ethylene/ethane adsorption selectivity, far surpassing benchmark zeolite and any other MOF and POP reported thus far. The formation of π-complexation between ethylene molecules and Ag(I) ions in PAF-1-SO_3Ag has been proven by heat of adsorption analysis and in situ IR spectroscopic studies.

RESULTS AND DISCUSSION

Materials Preparation and Physicochemical Characterization. PAF-1[22] [(cross-linked poly tetraphenylmethane) also known as (a.k.a.) PPN-6[23]] is an amorphous POP possessing a hypothetical diamondoid-topology structure with very high surface area and exceptional stability in water/moisture and acidic/basic media. PAF-1-SO_3Ag can be readily achieved by Ag(I) ion exchange of sulfonate-grafted PAF-1 (hereafter denoted PAF-1-SO_3H) following the procedures reported previously (Supporting Information (SI) Scheme S1).[23a,24a]

N_2 gas sorption isotherms at 77 K (Figure 1) reveal Brunauer−Emmett−Teller (BET) surface areas of 4714, 1087, and 783 $m^2 \cdot g^{-1}$ for PAF-1, PAF-1-SO_3H, and PAF-1-SO_3Ag, respectively. Pore size distribution analysis (Horvath−Kawazoe model) indicates that the pore size is reduced from ~15 Å for PAF-1 to ~8 Å for PAF-1-SO_3H, whereas the pore size of PAF-1-SO_3Ag is predominantly distributed around ~8 Å, suggesting negligible pore size change after the Ag(I) ion exchange process (SI Figure S1).

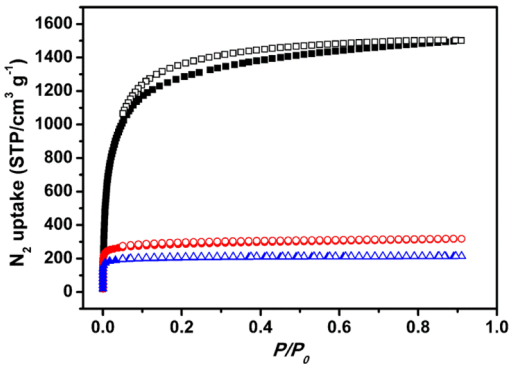

Figure 1. N_2 sorption isotherms at 77 K for PAF-1 (black), PAF-1-SO_3H (red), and PAF-1-SO_3Ag (blue).

The presence of Ag(I) in PAF-1-SO_3Ag was confirmed by X-ray photoelectron spectroscopy (XPS) analysis, which shows a silver signal at binding energies of 368.8 and 374.8 eV (SI Figure S2) corresponding to the peaks of Ag $3d_{5/2}$ and Ag $3d_{3/2}$, respectively. Fourier transform infrared spectroscopy (FTIR) of PAF-1-SO_3Ag shows the obvious characteristic peak of SO_3^- group at 1086 and 1186 cm^{-1}, respectively (SI Figure S3). Solid ^{13}C NMR spectra of PAF-1-SO_3Ag and PAF-1-SO_3H show similar central carbon atom signals at δ = 65 ppm and the signals of aromatic carbon (δ = 121 ppm to 147 ppm), indicating the preservation of framework structure after Ag(I) ion exchange (SI Figure S4). Inductively coupled plasma mass spectrometry (ICP-MS) and elemental analysis (EA) indicate that ~50% SO_3H were exchanged into SO_3Ag.

Ethylene and Ethane Adsorption. The low-pressure ethylene sorption isotherms were collected at 296 K. The incorporation of Ag(I) ion into PAF-1 results in a significant enhancement of ethylene adsorption capacity despite the remarkable decrease in surface area. At 296 K and 1 atm, the ethylene uptake amounts of PAF-1 and PAF-1-SO_3H are 57 and 66 $cm^3 \cdot g^{-1}$, respectively (SI Figure S5). In contrast, PAF-1-SO_3Ag exhibits a significantly higher ethylene uptake capacity of 91 $cm^3 \cdot g^{-1}$ (4.1 $mmol \cdot g^{-1}$) under the same conditions (Figure 2). PAF-1-SO_3Ag surpasses the ethylene uptake capacity of zeolite 5A[25] (~2.3 $mmol \cdot g^{-1}$ at 303 K and 1 atm) and compares to that of zeolite NaX[26] (~4.2 $mmol \cdot g^{-1}$ at 305 K and 1 atm), two benchmark zeolites widely studied for ethylene/ethane separation. In addition, PAF-1-SO_3Ag outperforms the copper(catecholate) decorated POP, $CuA_{10}B_1$,[20] in ethylene uptake, which exhibits an ethylene adsorption amount

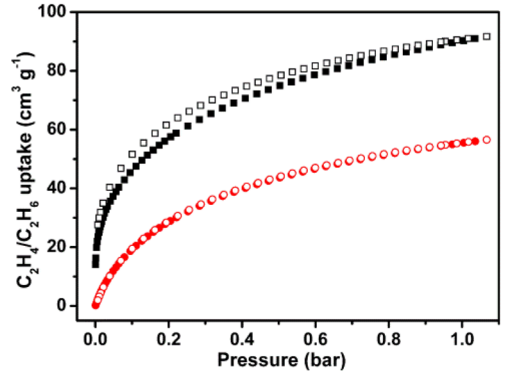

Figure 2. C_2H_4 (black) and C_2H_6 (red) sorption isotherms of PAF-1-SO_3Ag at 296 K. Filled: adsorption; unfilled: desorption.

dx.doi.org/10.1021/ja502119z | J. Am. Chem. Soc. 2014, 136, 8654−8660

of ~1.8 mmol·g^{-1} at 0.79 atm and 298 K. The ethylene uptake capacity of PAF-1-SO_3Ag at 296 K and 1 atm is relatively lower compared to that of some high surface area MOFs possessing open metal sites (e.g., 7.2 mmol·g^{-1} of MgMOF-74, 7.2 mmol·g^{-1} of Cu-BTC, and 5.8 mmol·g^{-1} of NOTT-102),[19a] but the MOFs containing open metal sites usually experience partial framework degradation after exposed to moisture, inevitably leading to drastic decreases in ethylene uptake capacity upon reuse. In contrast, the fact that PAF-1-SO_3Ag was prepared via ion exchange in aqueous solution suggests its water stability. This, together with its moisture stability, is further confirmed by the reproducibility of the ethylene sorption isotherms for PAF-1-SO_3Ag even after exposure to an air environment with 80% humidity for 2 days (SI Figure S6).

To test the recyclability of PAF-1-SO_3Ag, we simulated temperature and vacuum swings with an ASAP2020 analyzer, by saturating with ethylene up to 1.1 bar at 296 K followed by a high vacuum for 3 h at 105 °C. After 5 cycles, there was no apparent loss in capacity (SI Figure S7), indicating the complete desorption during each regeneration cycle. Upon the basis of the differential scanning calorimetry (DSC) analysis, energies of 2.67 MJ/kg are needed to release ethylene and regenerate PAF-1-SO_3Ag (SI Figure S8).[19b]

Interestingly, different from the ethylene adsorption, the trend of ethane uptake by the three samples follows the order of PAF-1 > PAF-1-SO_3H > PAF-1-SO_3Ag at 296 K and 1 atm (SI Figure S9). The smallest ethane uptake amount observed for PAF-1-SO_3Ag is primarily attributed to its lower surface area when compared with PAF-1 and PAF-1-SO_3H. This result also suggests that the incorporation of Ag(I) ions would not increase the ethane uptake capacity.

Ethylene/ethane adsorption selectivities were calculated using ideal adsorbed solution theory (IAST)[27] for PAF-1-SO_3Ag, PAF-1, and PAF-1-SO_3H (Figure 3). For an equimolar

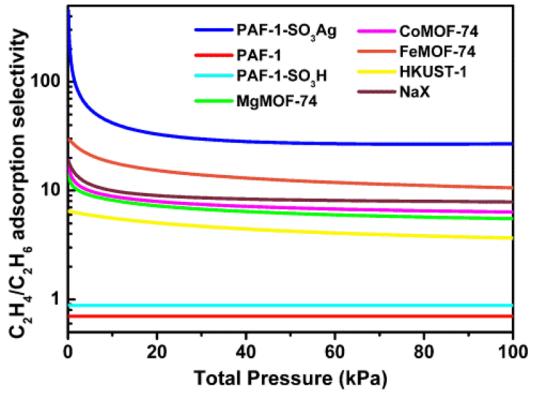

Figure 3. Comparison of the IAST calculations for C_2H_4/C_2H_6 adsorption selectivities for PAF-1-SO_3Ag with PAF-1, PAF-1-SO_3H and other porous materials[19a] at 296 K.

mixture of ethylene and ethane at 296 K, the adsorption selectivity (S_{ads}) obtained for PAF-1-SO_3Ag is 27 at 100 kPa, far exceeding those calculated for both PAF-1 (S_{ads} = 0.7) and PAF-1-SO_3H (S_{ads} = 0.88). The ethylene/ethane adsorption selectivity of PAF-1-SO_3Ag at 296 K and 100 kPa is also significantly higher than those of zeolite NaX,[19a] the MOFs[19a] FeMOF-74 [a.k.a. Fe_2(dobdc)], CoMOF-74 [a.k.a. Co_2(dobdc)], MgMOF-74 [a.k.a. Mg_2(dobdc)], CuBTC (a.k.a. HKUST-1) (Figure 3), and the POP $CuA_{10}B_1$,[20] exhibiting ethylene/ethane selectivities of 8, 11, 6.4, 5.6, 3.6, and 3.8, respectively. It is worth noting that the ethylene/ethane adsorption selectivities of PAF-1-SO_3Ag are considerably higher than those of zeolite NaX and other MOFs over the entire pressure range with the adsorption selectivity value at 1 kPa (S_{ads} = 125) even about an order of magnitude higher (Figure 3).

In practice, the combination of adsorption selectivity and uptake capacity of gas mixtures contribute to the characteristics of ethylene/ethane separation.[18c,19a] Figure 4 shows the IAST

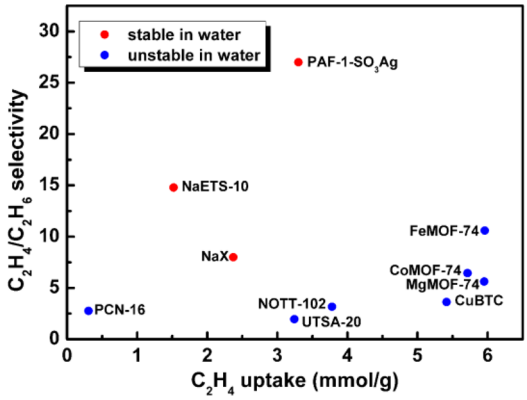

Figure 4. IAST calculations of the C_2H_4/C_2H_6 adsorption selectivity versus the gravimetric uptake capacity of ethylene for adsorption from an equimolar C_2H_4/C_2H_6 mixture at the total bulk gas phase at 296 K and 100 kPa[19a] (Note: the uptake capacity of ethylene for FeMOF-74 is at 318 K[19b]).

calculations of the ethylene/ethane adsorption selectivity versus the gravimetric uptake capacity of ethylene for adsorption from an equimolar ethylene/ethane mixture at the total bulk gas phase at 296 K and 100 kPa for PAF-1-SO_3Ag and several benchmark microporous adsorbent materials.[19a] Both adsorption selectivity and gravimetric uptake capacity of PAF-1-SO_3Ag are significantly higher than two important zeolites of NaETS-10[28] and NaX.[19a,29] The volumetric ethylene uptake capacity of PAF-1-SO_3Ag (SI Figure S11), which is estimated based on the density of the compressed PAF-1-SO_3Ag pellet, also surpasses that of NaETS-10[28] and NaX.[19a,29] Albeit the ethylene uptake capacity of PAF-1-SO_3Ag is lower than that of some MOF materials, much higher ethylene adsorption selectivity alongside excellent water stability represent advantages in practice over most MOFs[30] investigated so far.

Ethylene–Framework Interactions. We reasoned that the exceptional ethylene adsorption properties of PAF-1-SO_3Ag should stem from the strong interactions between ethylene molecules and the framework of PAF-1-SO_3Ag as a result of the formation of π-complexation between the *d* orbitals of Ag(I) and the π orbitals of carbon–carbon double bonds in ethylene.[5,6] We estimated the isosteric heats of adsorption (Q_{st}) based upon Clausius–Clapeyron equation by differentiation of the dual-Langmuir–Freundlich fits of the isotherms at two different temperatures,[18c,19a] 296 and 318 K(SI Figure S12) with *T*-dependent parameters. As shown in Figure 5, at close to zero loading, the Q_{st} for ethylene in PAF-1-SO_3Ag is 106 kJ·mol^{-1}, remarkably higher than that of PAF-1 (14 kJ·mol^{-1}) and PAF-1-SO_3H (23 kJ·mol^{-1}). The Q_{st} for ethylene in PAF-1-SO_3Ag is consistent with that observed in other Ag(I)-based π-complexation systems,[21,31] suggesting the formation of π-complexation between the ethylene molecules and Ag(I) ions in PAF-1-SO_3Ag. The Q_{st} exceeds that in MOFs with open

dx.doi.org/10.1021/ja502119z | J. Am. Chem. Soc. 2014, 136, 8654–8660

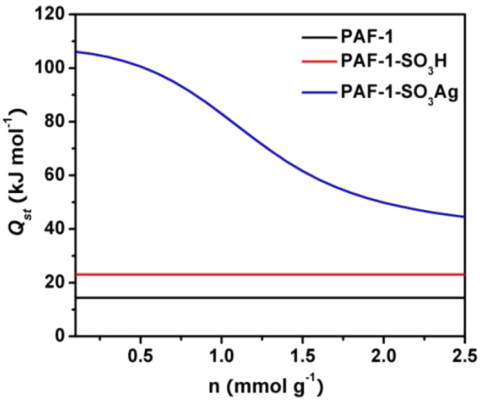

Figure 5. Isosteric heats adsorption, Q_{st} of C_2H_4 for PAF-1, PAF-1-SO_3H, and PAF-1-SO_3Ag.

metal sites, e.g., FeMOF-74 (45 kJ·mol^{-1})[19b] or (47 kJ·mol^{-1}),[19a] MgMOF-74 (42 kJ·mol^{-1}),[19a] CoMOF-74 (41 kJ·mol^{-1}),[19a] CuBTC (39 kJ·mol^{-1}).[19a] These results highlight that, compared with open metal sites, Ag(I) ions can boost the interactions with ethylene molecules more in a porous framework via the formation of π-complexation. In contrast with the high Q_{st} for ethylene, PAF-1-SO_3Ag shows a significantly lower Q_{st} for ethane with a value of 27 kJ·mol^{-1} (SI Figure S14); thus validating that the Ag(I) ions serve as a preferential binding sites, selectively adsorbing ethylene over ethane thereby resulting in high ethylene/ethane adsorption selectivities.

To further prove the formation of π-complexation between the ethylene molecules and Ag(I) ions in PAF-1-SO_3Ag, in situ IR measurements of ethylene adsorption at room temperature were conducted. The —CH_2 out-of plane wagging mode at 949 cm^{-1} was found as the most sensitive mode, responding to the interaction between ethylene and the substrate surface.[32] As shown in Figure 6, ethylene adsorption on PAF-1 and PAF-1-

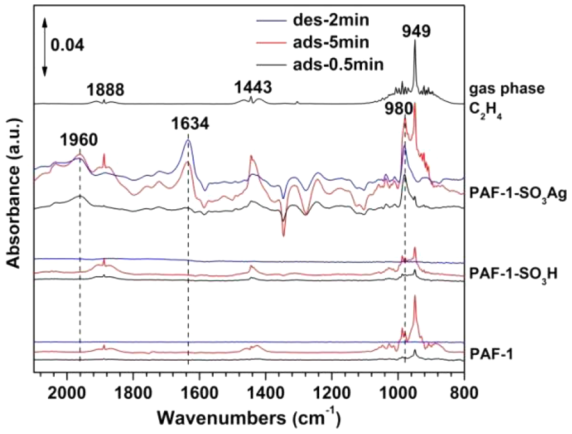

Figure 6. IR spectra from ethylene adsorption and desorption on PAF-1, PAF-1-SO_3H, and PAF-1-SO_3Ag at room temperature. IR spectrum from gas phase ethylene is also shown for reference.

SO_3H exhibits IR features similar to that of gas phase C_2H_4, indicating a weak interaction, which is further evidenced by the complete removal of ethylene IR features after room temperature desorption in helium purge. In contrast, upon initial adsorption, PAF-1-SO_3Ag shows strongly perturbed CH_2 mode at 980 cm^{-1}. The intensity is even comparable with the gas-phase mode at 949 cm^{-1} at saturation. Two extra IR features at 1960 cm^{-1} (combination mode of —CH_2 wagging) and 1634 cm^{-1} (C═C stretching), not observed on the PAF-1 and PAF-1-SO_3H, further confirm ethylene adsorption on PAF-1-SO_3Ag. These new IR bands due to adsorbed ethylene persist well after room temperature desorption, indicating a strong interaction between ethylene and PAF-1-SO_3Ag. The blue-shift of the —CH_2 wagging mode can be attributed to the combinative d−π and d−π* interaction between Ag and ethylene,[33−36] thus confirming the formation of π-complexation between the ethylene and Ag(I) ions in PAF-1-SO_3Ag.

Ethylene/Ethane Breakthrough Experiments and Simulations. To evaluate the performance of PAF-1-SO_3Ag in an actual adsorption-based separation process, breakthrough experiments were performed in which an equimolar ethylene/ethane mixture was flowed over a packed bed of the solid with a total flow of 2 mL/min at 296 K. As shown in Figure 7, PAF-1-SO_3Ag can effectively separate an equimolar mixture of ethylene and ethane into the pure component gases of greater than 99% purity.

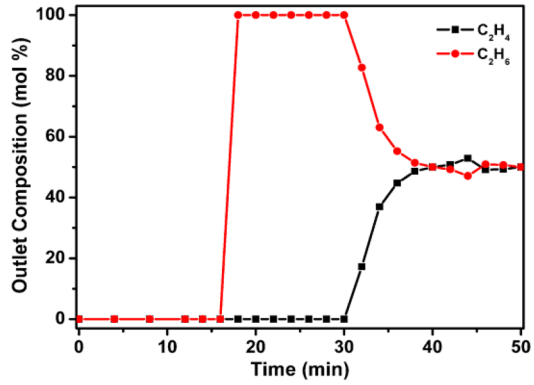

Figure 7. Experimental data on transient breakthrough of an equimolar C_2H_4/C_2H_6 mixture in an adsorber bed packed with PAF-1-SO_3Ag in the adsorption phase of a PSA operation.

We also carried out breakthrough simulations for C_2H_4/C_2H_6 mixtures in a fixed bed (SI Figure S17) to further demonstrate the feasibility of producing 99.95%+ pure C_2H_4 in a Pressure Swing Adsorption (PSA) operation. The simulated breakthrough curves are in reasonably good agreement with the experimental data (SI Figure S18a). During the adsorption cycle, C_2H_6 at purities >99% can be recovered for a certain duration of the adsorption cycle, as indicated by the arrow in SI Figure S18b. In addition, ethylene of 99.95%+ purity, required as feedstock to the polymerization reactor, can also be recovered during the time interval indicated by the arrow in SI Figure S19 in the desorption cycle. Video animations of the breakthrough simulations can be viewed in the HTML version of this work.

■ CONCLUSIONS

In summary, we have demonstrated for the first time the introduction of π-complexation into POPs for highly selective adsorption of ethylene over ethane, as illustrated in the context of Ag(I) ion functionalized porous aromatic framework, PAF-1-SO_3Ag. PAF-1-SO_3Ag exhibits significantly higher ethylene/ethane adsorption selectivity at 296 K than benchmark zeolite and any other MOF and POP reported in literature. The high ethylene/ethane adsorption selectivity of PAF-1-SO_3Ag is traceable to the formation of π-complexation between Ag(I)

dx.doi.org/10.1021/ja502119z | J. Am. Chem. Soc. 2014, 136, 8654−8660

ions and the double bonds of ethylene molecules, which is reflected in the high isosteric heats of adsorption of C_2H_4 and evidenced by in situ IR spectroscopy studies. The feasibility of PAF-1-SO_3Ag for producing 99.95%+ pure C_2H_4 in a PSA operation has been demonstrated by breakthrough experiments that are supported by simulations. Albeit the light-sensitivity, utilization of costly Ni-COD catalyst, and high isosteric heats of adsorption could represent some potential challenges for the application of PAF-1-SO_3Ag in practice, these kinds of issues could be tackled via some engineering processes. Notwithstanding, our work presented herein provides a new perspective to functionalizing POPs for energy-saving ethylene/ethane and other olefin/paraffin separations. Ongoing work in our laboratory includes investigating PAF-1-SO_3Ag for separations of other olefin/paraffin mixtures and applying the approach of π-complexation to functionalizing other types of advanced porous materials for hydrocarbon separations.

EXPERIMENTAL SECTION

Materials and Syntheses. All starting materials, reagents, and solvents were purchased from commercial sources (Aldrich, Alfa, Fisher, and Acros) and used without further purification.

Synthesis of Tetrakis(4-bromophenyl)methane. Tetrakis(4-bromophenyl)methane was synthesized according to the procedures reported in the literature[22] with some minor modification. To a three-necked round-bottom flask containing bromine (6.4 mL, 19.9 g), tetraphenylmethane (2.0 g, 6.24 mmol) was added stepwise with small portions under vigorous stirring at room temperature (25 °C). After the addition was completed, the resulting solution was stirred for 60 min and then cooled to 0 °C. At 0 °C temperature, ethanol (25 mL) was added slowly, and the reaction mixture was allowed to warm to room temperature overnight. Then, the precipitate was filtered off and washed subsequently with saturated aqueous sodium hydrogensulfite solution (25 mL) and water (100 mL). After drying at 80 °C for 24 h under vacuum (80 mbar), tetrakis(4-bromophenyl) methane was recrystallized in EtOH/CH_2Cl_2 to afford a yellow solid, yield: 88%.

Synthesis of PAF-1. PAF-1 was synthesized according to the procedures reported in the literature[23a] with some minor modification. Tetrakis(4-bromophenyl)methane (509 mg, 0.8 mmol) was added to a solution of 2,2′-bipyridyl (565 mg, 3.65 mmol), bis(1,5-cyclooctadiene)nickel(0) (1.0 g, 3.65 mmol), and 1,5-cyclooctadiene (0.45 mL, 3.65 mmol) in anhydrous DMF/THF (60 mL/90 mL), and the mixture was stirred overnight at room temperature under nitrogen atmosphere. After the reaction, 6 M HCl (60 mL) was added slowly, and the resulting mixture was stirred for 12 h. The precipitate was collected by filtration, then washed with methanol and water, and dried at 150 °C for 24 h under vacuum (80 mbar) to produce PAF-1 as a white powder, yield: 80%.

Synthesis of PAF-1-SO_3H. PAF-1-SO_3H was synthesized according to the procedures reported in the literature[23a,24] with some minor modification. To an ice-cooled mixture of PAF-1 (100 mg) in dichloromethane (15 mL), chlorosulfonic acid (1.0 mL) was added dropwise. The resulting mixture was stirred at room temperature for 3 days. Then, the mixture was poured over ice, and the solid was collected, washed with water thoroughly, and dried 150 °C for 24 h under vacuum (80 mbar) to produce PAF-1-SO_3H as blue powder, yield: 96%.

Synthesis of PAF-1-SO_3Ag. To the 15 mL CH_3CN/H_2O (1:1) solution, 100 mg PAF-1-SO_3H and 800 mg $AgBF_4$ were added. The mixture was stirred under room temperature for 48 h, and then the solid was collected by filtration followed by washing with CH_3CN and water. The whole process was performed carefully under dark environment. This exchange process was repeated three times, and then dried at 110 °C under vacuum (80 mbar) for further test, yield: 94%. EA: C: 47.25%; H: 3.19%; N: 0.53%; S: 17.11%; ICP-MS: Ag: 29.20%.

Gas Adsorption. Gas sorption measurements were performed using an ASAP 2020 volumetric adsorption analyzer. High-purity grade gases of N_2 (99.999%), C_2H_4 (99.5%), and C_2H_6 (99.5%) were used for the collection of respective sorption isotherms.

In Situ IR Experiments. IR spectra of ethylene adsorption were collected using a Thermo Nicolet Nexus 670 spectrometer in diffuse reflectance mode (DRIFTS). The PAF-1-SO_3Ag sample, ca. 5 mg, was treated in a DRIFTS cell (HC-900, Pike Technologies) at 423 K in helium (30 mL/min) for 1 h to removal water and other adsorbates. The sample was then cooled down to room temperature for ethylene adsorption. The adsorption was conducted by flowing 10% ethylene/He (30 mL/min) over the sample for 5 min and then desorption was done in flowing helium. IR spectra were recorded continuously to follow the surface changes during the adsorption and desorption process. All reported IR spectra are difference spectra referenced to a background spectrum collected at room temperature after pretreatment but prior to ethylene adsorption.

Fitting of Pure Component Isotherms. The measured experimental isotherm data for C_2H_4, and C_2H_6 on PAF-1-SO_3Ag were fitted with the dual-Langmuir−Freundlich isotherm model:

$$q = q_{A,sat}\frac{b_A p^{\nu_A}}{1 + b_A p^{\nu_A}} + q_{B,sat}\frac{b_B p^{\nu_B}}{1 + b_B p^{\nu_B}} \quad (1)$$

The fit parameters for C_2H_4 and C_2H_6 are specified in SI Table S1. SI Figure S13 presents a comparison of the experimentally determined component loadings for C_2H_4 and C_2H_6 on PAF-1-SO_3Ag at 296 K with the isotherm fits using parameters specified in SI Table S1. The fits are excellent over the entire range of pressures.

The pure component isotherm data for PAF-1, and PAF-1-SO_3H could be fitted with single site Langmuir model; the fit parameters are provided in SI Tables S2 and S3, respectively.

Calculations of Adsorption Selectivity. The selectivity of preferential adsorption of C_2H_4 (component 1) over C_2H_6 (component 2) in a mixture containing 1 and 2, can be formally defined as follows:

$$S_{ads} = \frac{q_1/q_2}{p_1/p_2} \quad (2)$$

In eq 2, q_1 and q_2 are the component loadings of the adsorbed phase in the mixture. The calculations of S_{ads} are based on the use of the Ideal Adsorbed Solution Theory (IAST) of Myers and Prausnitz.[27]

Estimation of Isosteric Heats of Adsorption, Q_{st}. The isosteric heat of adsorption, Q_{st}, were calculated using the Clausius−Clapeyron equation by differentiation of the dual-Langmuir−Freundlich fits of the isotherms at two different temperatures, 296 and 318 K with T-dependent parameters.

$$Q_{st} = RT^2\left(\frac{\partial \ln p}{\partial T}\right)_q \quad (3)$$

Breakthrough Experiments. In a typical experiment, 400 mg of PAF-1-SO_3Ag was swiftly ground and packed into a quartz column (6 mm I.D. × 220 mm) with silica wool filling the void space. The sample was in situ activated under vacuum (6.5×10^{-4} Pa) at 110 °C for 2 h. Then, Helium flow (2 mL/min) was introduced the system to purge the adsorbent until the temperature of the column was decreased to 23 °C. The breakthrough test was started by introducing a 1:1 C_2H_4/C_2H_6 mixture gas at a total flow rate of 2.0 mL/min and switching off the He gas. Effluent from the column was monitored using a GC with a flame ionization detector. The dead volume of this setup was determined to be 18.6 cm^3.

ASSOCIATED CONTENT

Supporting Information

Characterization details, additional gas sorption isotherms, simulated breakthrough curves, TGA plots, XPS and IR spectra plots, and supporting figures. This material is available free of charge via the Internet at http://pubs.acs.org.

Web-Enhanced Feature

Video animations of transient breakthrough for the adsorption/desorption cycle are available in the HTML version of this paper.

AUTHOR INFORMATION

Corresponding Author

sqma@usf.edu

Notes

The authors declare no competing financial interest.

ACKNOWLEDGMENTS

The authors acknowledge the University of South Florida for financial support of this work, and an award from the National Science Foundation (DMR-1352065) is also acknowledged. Part of the work including the in situ IR studies was conducted at the Center for Nanophase Materials Sciences, which is sponsored at Oak Ridge National Laboratory by the Scientific User Facility Division, Office of Basic Energy Sciences (BES), U.S. Department of Energy (DOE). DOE/BES/Division of Materials Sciences and Engineering (Award No. KC020105-FWP12152) (P.K.T.) and the National Natural Science Foundation of China (No. 21371069) (Z.S.) are acknowledged. We thank Prof. Jeffrey R. Long and Eric Bloch for their kind help on the calculation of regeneration energies.

REFERENCES

(1) Matar, S.; Hatch, L. F. *Chemistry of Petrochemical Processes*, 2nd ed.; Gulf Publishing Company: Texas, 2000.

(2) Eldridge, R. B. *Ind. Eng. Chem. Res.* **1993**, *32*, 2208.

(3) Rege, S. U.; Padin, J.; Yang, R. T. *AIChE J.* **1998**, *44*, 799.

(4) Zhu, X.; Tian, C.; Mahurin, S. M.; Chai, S.-H.; Wang, C.; Brown, S.; Veith, G. M.; Luo, H.; Liu, H.; Dai, S. *J. Am. Chem. Soc.* **2012**, *134*, 104784.

(5) Safarik, D. J.; Eldridge, R. B. *Ind. Eng. Chem. Res.* **1998**, *37*, 2571.

(6) Yang, R. T. *Adsorbents: Fundamentals and Applications*; John Wiley & Sons, Inc.: NJ, 2003.

(7) (a) MacGillivray, L. R. *Metal-Organic Frameworks: Design and Application*; John Wiley & Sons: Hoboken, NJ, 2010. (b) Zhou, H.-C.; Long, J. R.; Yaghi, O. M. *Chem. Rev.* **2012**, *112*, 673. (c) Cohen, S. M. *Chem. Rev.* **2012**, *112*, 970. (d) Kitagawa, S.; Kitaura, R.; Noro, S.-I. *Angew. Chem., Int. Ed.* **2004**, *43*, 2334. (e) Cook, T. R.; Zheng, Y.-R.; Stang, P. J. *Chem. Rev.* **2013**, *113*, 734.

(8) (a) Thomas, A. *Angew. Chem., Int. Ed.* **2010**, *49*, 8328. (b) Dawson, R.; Cooper, A. I.; Adams, D. J. *Prog. Polym. Sci.* **2012**, *37*, 530. (c) Xu, Y.; Jin, S.; Xu, H.; Nagai, A.; Jiang, D. *Chem. Soc. Rev.* **2013**, *42*, 8012.

(9) (a) Ben, T.; Qiu, S. *CrystEngComm* **2013**, *15*, 17. (b) Zou, X.; Ren, H.; Zhu, G. *Chem. Commun.* **2013**, *49*, 3925.

(10) (a) Cooper, A. I. *Adv. Mater.* **2009**, *21*, 1291. (b) Schwab, M. G.; Fassbender, B.; Spiess, H. W.; Thomas, A.; Feng, X.; Mullen, K. *J. Am. Chem. Soc.* **2009**, *131*, 7216. (c) Spitler, E. L.; Dichtel, W. R. *Nat. Chem.* **2010**, *2*, 672.

(11) (a) Lu, W.; Yuan, D.; Zhao, D.; Schilling, C. I.; Plietzsch, O.; Muller, T.; Brase, S.; Guenther, J.; Blumel, J.; Krishna, R.; Li, Z.; Zhou, H.-C. *Chem. Mater.* **2010**, *22*, 5964. (b) Yuan, D.; Lu, W.; Zhao, D.; Zhou, H.-C. *Adv. Mater.* **2011**, *23*, 3723.

(12) (a) Yuan, S.; Dorney, B.; White, D.; Kirklin, S.; Yu, L.; Liu, D.-J. *Chem. Commun.* **2010**, *46*, 4547. (b) Weston, M. H.; Farha, O. K.; Hauser, B. G.; Hupp, J. T.; Nguyen, S. T. *Chem. Mater.* **2012**, *24*, 1292.

(13) (a) Ma, S.; Zhou, H.-C. *Chem. Commun.* **2010**, *46*, 44. (b) Suh, M. P.; Park, H. J.; Prasad, T. K.; Lim, D.-W. *Chem. Rev.* **2012**, *112*, 782. (c) Rabbani, M. G.; El-Kaderi, H. M. *Chem. Mater.* **2012**, *24*, 1511. (d) Wood, C. D.; Tan, B.; Trewin, A.; Su, F.; Rosseinsky, M. J.; Bradshaw, D.; Sun, Y.; Zhou, L.; Cooper, A. I. *Adv. Mater.* **2008**, *20*, 1916.

(14) (a) Li, J.-R.; Sculley, J.; Zhou, H.-C. *Chem. Rev.* **2012**, *112*, 869. (b) Zhu, Y.; Long, H.; Zhang, W. *Chem. Mater.* **2013**, *25*, 1630. (c) Sato, H.; Kosaka, W.; Matsuda, R.; Hori, A.; Hijikata, Y.; Belosludov, R. V.; Sakaki, S.; Takata, M.; Kitagawa, S. *Science* **2014**, *343*, 167.

(15) (a) Liu, J.; Thallapally, P. K.; McGrail, B. P.; Brown, D. R.; Liu, J. *Chem. Soc. Rev.* **2012**, *41*, 2308. (b) Nugent, P.; Belmabkhout, Y.; Burd, S. D.; Cairns, A. J.; Luebke, R.; Forrest, K.; Pham, T.; Ma, S.; Space, B.; Wojtas, L.; Eddaoudi, M.; Zaworotko, M. J. *Nature* **2013**, *495*, 80. (c) Sumida, K.; Rogow, D. L.; Mason, J. A.; McDonald, T. M.; Bloch, E. D.; Herm, Z. R.; Bae, T.-H.; Long, J. R. *Chem. Rev.* **2012**, *112*, 724. (d) Dawson, R.; Stöckel, E.; Holst, J. R.; Adams, D. J.; Cooper, A. I. *Energy Environ. Sci.* **2011**, *4*, 4239−4245. (e) An, J.; Rosi, N. L. *J. Am. Chem. Soc.* **2010**, *132*, 5578.

(16) (a) Gu, X.; Lu, Z.-H.; Jiang, H.-L.; Akita, T.; Xu, Q. *J. Am. Chem. Soc.* **2011**, *133*, 11822. (b) Yoon, M.; Srirambalaji, R.; Kim, K. *Chem. Rev.* **2012**, *112*, 1196. (c) Lee, J.; Farha, O. K.; Roberts, J.; Scheidt, K. A.; Nguyen, S. T.; Hupp, J. T. *Chem. Soc. Rev.* **2009**, *38*, 1450. (d) Corma, A.; García, H.; Llabrés i Xamena, F. X. *Chem. Rev.* **2010**, *110*, 4606. (e) Shultz, A. M.; Farha, O. K.; Hupp, J. T.; Nguyen, S. T. *Chem. Sci.* **2011**, *2*, 686. (f) Chen, L.; Yang, Y.; Jiang, D. *J. Am. Chem. Soc.* **2010**, *132*, 9138. (g) Chen, L.; Yang, Y.; Guo, Z.; Jiang, D. *Adv. Mater.* **2011**, *23*, 3149. (h) Lykourinou, V.; Chen, Y.; Wang, X.-S.; Meng, L.; Hoang, T.; Ming, L.-J.; Musselman, R. L.; Ma, S. *J. Am. Chem. Soc.* **2011**, *133*, 10382. (i) Meng, L.; Cheng, Q.; Kim, C.; Gao, W.-Y.; Wojtas, L.; Cheng, Y.-S.; Zaworotko, M. J.; Zhang, X. P.; Ma, S. *Angew. Chem. Int. Ed.* **2012**, *51*, 10082. (j) Li, B.; Zhang, Y.; Ma, D.; Ma, T.; Shi, Z.; Ma, S. *J. Am. Chem. Soc.* **2014**, *136*, 1202. (k) Gao, W.-Y.; Chen, Y.; Niu, Y.; Williams, K.; Cash, L.; Perez, P. J.; Wojtas, L.; Cai, J.; Chen, Y.-S.; Ma, S. *Angew. Chem. Int. Ed.* **2014**, *53*, 2615. (l) Zhu, C.; Yuan, G.; Chen, X.; Yang, Z.; Cui, Y. *J. Am. Chem. Soc.* **2012**, *134*, 8058.

(17) Davis, M. E. *Nature* **2002**, *417*, 813.

(18) (a) Wu, H.; Gong, Q.; Olson, D. H.; Li, J. *Chem. Rev.* **2012**, *112*, 836. (b) Xiang, S.-C.; Zhang, Z.; Zhao, C.-G.; Hong, K.; Zhao, X.; Ding, D.-R.; Xie, M.-H.; Wu, C.-D.; Das, M. C.; Gill, R.; Mark Thomas, K.; Chen, B. *Nat. Commun.* **2011**, *2*, 204. (c) Krishna, R. *Microporous Mesoporous Mater.* **2014**, *185*, 30. (d) Lee, C. Y.; Bae, Y.-S.; Jeong, N. C.; Farha, O. K.; Sarjeant, A. A.; Stern, C. L.; Nickias, P.; Snurr, R. Q.; Hupp, J. T.; Nguyen, S. T. *J. Am. Chem. Soc.* **2011**, *133*, 5228. (e) Bae, Y.-S.; Lee, C. Y.; Kim, K. C.; Farha, O. K.; Nickias, P.; Hupp, J. T.; Nguyen, S. T.; Snurr, R. Q. *Angew. Chem., Int. Ed.* **2012**, *51*, 1857. (f) Li, K.; Olson, D. H.; Seidel, J.; Emge, T. J.; Gong, H.; Zeng, H.; Li, J. *J. Am. Chem. Soc.* **2009**, *131*, 10368. (g) Nijem, N.; Wu, H.; Canepa, P.; Marti, A.; Balkus, K. J., Jr.; Thonhauser, T.; Li, J.; Chabal, Y. J. *J. Am. Chem. Soc.* **2012**, *134*, 15201. (h) Maes, M.; Alaerts, L.; Vermoortele, F.; Ameloot, R.; Couck, S.; Finsy, V.; Denayer, J. F. M.; De Vos, D. E. *J. Am. Chem. Soc.* **2010**, *132*, 2284. (i) Lamia, N.; Jorge, M.; Granato, M. A.; AlmeidaPaz, F. A.; Chevreau, H.; Rodrigues, A. E. *Chem. Eng. Sci.* **2009**, *64*, 3246. (j) Ferreira, A. F. P.; Santos, J. C.; Plaza, M. G.; Lamia, N.; Loureiro, J. M.; Rodrigues, A. E. *Chem. Eng. J.* **2011**, *167*, 1. (k) Yoon, J. W.; Seo, Y.-K.; Hwang, Y. K.; Chang, J.-S.; Leclerc, H.; Wuttke, S.; Bazin, P.; Vimont, A.; Daturi, M.; Bloch, E.; Llewellyn, P. L.; Serre, C.; Horcajada, P.; Grenèche, J.-M.; Rodrigues, A. E.; Férey, G. *Angew. Chem., Int. Ed.* **2010**, *49*, 5949. (l) van den Bergh, J.; Gücüyener, C.; Pidko, E. A.; Hensen, E. J. M.; Gascon, J.; Kapteijn, F. *Chem.—Eur. J.* **2011**, *17*, 8832. (m) Cai, J.; Yu, J.; Xu, H.; He, Y.; Duan, X.; Cui, Y.; Wu, C.; Chen, B.; Qian, G. *Cryst. Growth Des.* **2013**, *13*, 2094. (n) Xu, H.; Cai, J.; Xiang, S.; Zhang, Z.; Wu, C.; Rao, X.; Cui, Y.; Yang, Y.; Krishna, R.; Chen, B.; Qian, G. *J. Mater. Chem. A* **2013**, *1*, 9916. (o) Leclerc, H.; Vimont, A.; Lavalley, J.-C.; Daturi, M.; Wiersum, A. D.; Llwellyn, P. L.; Horcajada, P.; Férey, G.; Serre, C. *Phys. Chem. Chem. Phys.* **2011**, *13*, 11748. (p) Uchida, S.; Eguchi, R.; Nakamura, S.; Ogasawara, Y.; Kurosawa, N.; Mizuno, N. *Chem. Mater.* **2012**, *24*, 325. (q) Rubeš, M.; Wiersum, A. D.; Llewellyn, P. L.; Grajciar, L.; Bludskyì, O.; Nachtigall, P. *J. Phys. Chem. C* **2013**, *117*, 11159. (r) Hartmann, M.; Kunz, S.; Himsl, D.; Tangermann, O. *Langmuir* **2008**, *24*, 8634. (s) He, Y.; Zhang, Z.; Xiang, S.; Fronczek, F. R.; Krishna, R.; Chen, B. *Chem.—Eur. J.* **2012**, *18*, 613. (t) Herm, Z.

R.; Bloch, E. D.; Long, J. R. *Chem. Mater.* **2013**, *26*, 323. (u) Ma, H.; Ren, H.; Meng, S.; Sun, F.; Zhu, G. *Sci. Rep.* **2013**, *3*, 2611. (v) Wang, X.-S.; Liu, J.; Bonefont, J. M.; Yuan, D.-Q.; Thallapally, P. K.; Ma, S. *Chem. Commun.* **2013**, *49*, 1533. (w) Das, M. C.; Guo, Q.; He, Y.; Kim, J.; Zhao, C.-G.; Hong, K.; Xiang, S.; Zhang, Z.; Mark Thomas, K.; Krishna, R.; Chen, B. *J. Am. Chem. Soc.* **2012**, *134*, 8703.

(19) (a) He, Y.; Krishna, R.; Chen, B. *Energy Environ. Sci.* **2012**, *5*, 9107. (b) Bloch, E. D.; Queen, W. L.; Krishna, R.; Zadrozny, J. M.; Brown, C. M.; Long, J. R. *Science* **2012**, *335*, 1606. (c) Geier, S. J.; Mason, J. A.; Bloch, E. D.; Queen, W. L.; Hudson, M. R.; Browncd, C. M.; Long, J. R. *Chem. Sci.* **2013**, *4*, 2054. (e) Gücüyener, C.; van den Bergh, J.; Gascon, J.; Kapteijn, F. *J. Am. Chem. Soc.* **2010**, *132*, 17704. (f) Böhme, U.; Barth, B.; Paula, C.; Kuhnt, A.; Schwieger, W.; Mundstock, A.; Caro, J.; Hartmann, M. *Langmuir* **2013**, *29*, 8592. (g) Bao, Z.; Alnemrat, S.; Yu, L.; Vasiliev, I.; Ren, Q.; Lu, X.; Deng, S. *Langmuir* **2011**, *27*, 13554. (h) Huang, L.; Cao, D. *J. Mater. Chem. A* **2013**, *1*, 9433.

(20) Weston, M. H.; Colón, Y. J.; Bae, Y.-S.; Garibay, S. J.; Snurr, R. Q.; Farha, O. K.; Hupp, J. T.; Nguyen, S. T. *J. Mater. Chem. A* **2014**, *2*, 299.

(21) Uchida, S.; Kawamoto, R.; Tagami, H.; Nakagawa, Y.; Mizuno, N. *J. Am. Chem. Soc.* **2008**, *130*, 12370.

(22) Ben, T.; Ren, H.; Ma, S.; Cao, D.; Lan, J.; Jing, X.; Wang, W.; Xu, J.; Deng, F.; Simmons, J. M.; Qiu, S.; Zhu, G. *Angew. Chem., Int. Ed.* **2009**, *48*, 9457.

(23) (a) Lu, W.; Yuan, D.; Sculley, J.; Zhao, D.; Krishna, R.; Zhou, H.-C. *J. Am. Chem. S oc.* **2011**, *133*, 18126. (b) Lu, W.; Sculley, J. P.; Yuan, D.; Krishna, R.; Wei, Z.; Zhou, H.-C. *Angew. Chem., Int. Ed.* **2012**, *51*, 7480.

(24) (a) Zhang, Y.; Li, B.; Williams, K.; Gao, W.-Y.; Ma, S. *Chem. Commun.* **2013**, *49*, 10269. (b) Van Humbeck, J. F.; McDonald, T. M.; Jing, X.; Wiers, B. M.; Zhu, G.; Long, J. R. *J. Am. Chem. Soc.* **2014**, *136*, 2432.

(25) Mofarahi, M.; Salehi, S. M. *Adsorption* **2013**, *19*, 101.

(26) Choudhary, V. R.; Mayadevi, S.; Singh, A. P. *J. Chem. Soc. Faraday Trans.* **1995**, *91*, 2935.

(27) Myers, A. L.; Prausnitz, J. M. *AIChE J.* **1965**, *11*, 121.

(28) Anson, A.; Wang, Y.; Lin, C. C. H.; Kuznicki, T. M.; Kuznicki, S. M. *Chem. Eng. Sci.* **2008**, *63*, 4171.

(29) Hyun, S. H.; Danner, R. P. *J. Chem. Eng. Data* **1982**, *27*, 196.

(30) (a) Liu, J.; Benin, A. I.; Furtado, A. M. B.; Jakubczak, P.; Willis, R. R.; LeVan, M. D. *Langmuir* **2011**, *27*, 11451. (b) Schoenecker, P. M.; Carson, C. G.; Jasuja, H.; Flemming, C. J. J.; Walton, K. S. *Ind. Eng. Chem. Res.* **2012**, *51*, 6513.

(31) (a) Yang, R. T.; Kikkinides, E. S. *AIChE J.* **1995**, *41*, 509. (b) Aguado, S.; Bergeret, G.; Daniel, C.; Farrusseng, D. *J. Am. Chem. Soc.* **2012**, *134*, 14635.

(32) Busca, G.; Lorenzelli, V.; Ramis, G.; Escribano, V. S. *Mater. Chem. Phys.* **1991**, *29*, 175.

(33) Stacchiola, D.; Wu, G.; Kaltchev, M.; Tysoe, W. T. *Surf. Sci.* **2001**, *486*, 9.

(34) Itoh, K.; Kiyohara, T.; Shinohara, H.; Ohe, C.; Kawamura, Y.; Nakai, H. *J. Phys. Chem. B* **2002**, *106*, 10714.

(35) Huang, Y. *J. Catal.* **1980**, *61*, 461.

(36) Uzunova, E. L.; Mikosch, H. *ACS Catal.* **2013**, *3*, 2759.

Supporting Information

Introduction of π-Complexation into Porous Aromatic Framework for Highly Selective Adsorption of Ethylene over Ethane

Baiyan Li,[†] Yiming Zhang,[†] Rajamani Krishna,[‡] Kexin Yao,[&] Yu Han,[&] Zili Wu,[§] Dingxuan Ma,[¶] Zhan Shi,[¶] Tony Pham,[†] Brian Space,[†] Jian Liu,[#] Praveen K. Thallapally,[#] Jun Liu,[#] Matthew Chrzanowski,[†] Shengqian Ma[†,*]

[†]Department of Chemistry, University of South Florida, 4202 E. Fowler Avenue, Tampa, FL 33620, USA.

[‡]Van't Hoff Institute for Molecular Sciences, University of Amsterdam, Science Park 904, 1098 XH Amsterdam, Netherlands.

[&]Advanced Membranes and Porous Materials Center, Physical Sciences and Engineering Division, King Abdullah University of Science and Technology, Thuwal 23955-6900, Kingdom of Saudi Arabia

[§]Center for Nanophase Materials Science and Chemical Science Division, Oak Ridge National Laboratory, TN 37831, USA.

[¶]State Key Laboratory of Inorganic Synthesis and Preparative Chemistry, College of Chemistry, Jilin University, Changchun 130012, People's Republic of China.

[#] Pacific Northwest National Laboratory, Richland, WA 99352, USA.

E-mail: sqma@usf.edu

Characterization Details

Elemental analyses were performed on a Perkin-Elmer 2400 element analyzer. Inductively coupled plasma (ICP) analysis was performed on a Perkin–Elmer Optima 3300DV spectrometer. IR spectra were recorded on a Nicolet Impact 410 FTIR spectrometer. XPS measurements were performed on an ESCALAB 250 X-ray photoelectron spectroscopy, using Mg Kα X-ray as the excitation source. Thermogravimetric analysis (TGA) was performed under nitrogen on a TA Instrument TGA 2950 Hi-Res. ^{13}C NMR were performed on a Bruker AVANCE IIIHD console with 1.9mm MAS probe. DSC analysis was performed on a TA Q20 analyzer, the ramping rate is 2 °C/min.

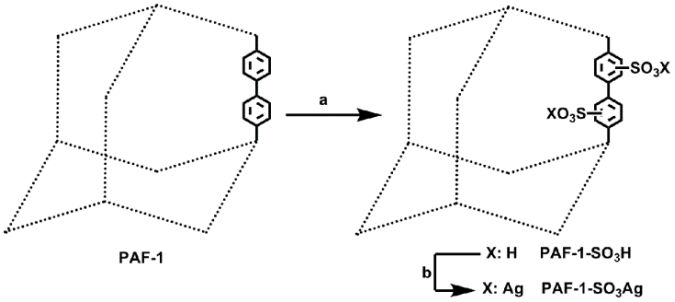

Scheme 1. Synthetic route of PAF-1-SO_3Ag. (a) CH_2Cl_2, $ClSO_3H$, 25 °C, 3 days; (b) $AgNO_3$, CH_3CN/H_2O, 3 times.

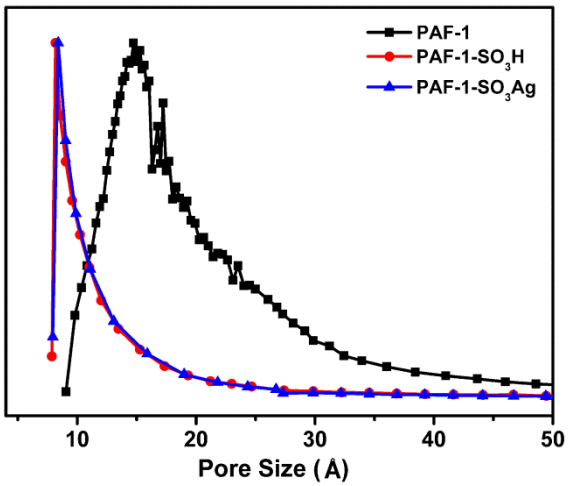

Figure S1. Pore size distribution of PAF-1, PAF-1-SO_3H, and PAF-1-SO_3Ag (Horvath–Kawazoe model).

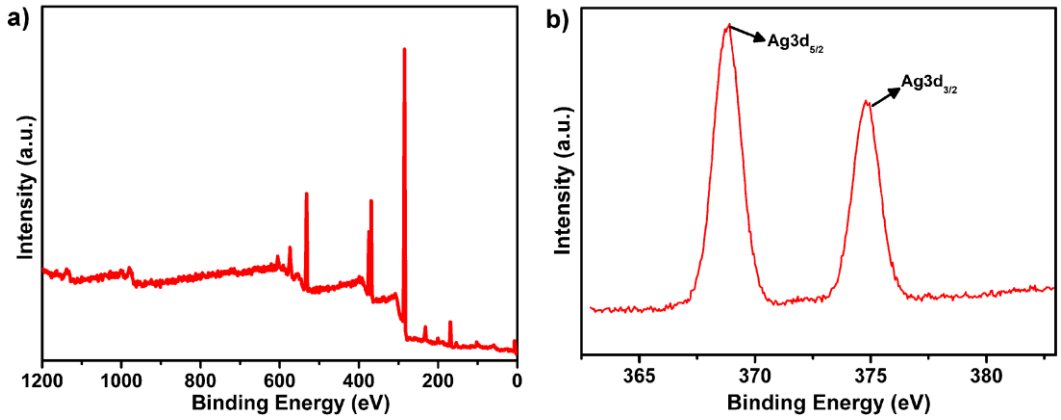

Figure S2. (a) XPS of PAF-1-SO_3Ag; (b) the enlarged XPS for Ag(I) sites.

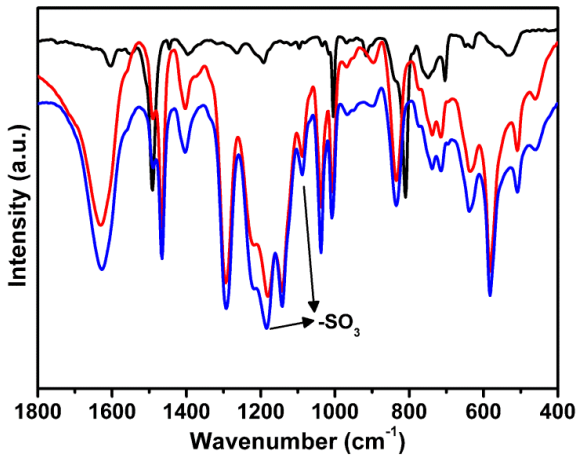

Figure S3. The IR spectra of PAF-1 (black), PAF-1-SO_3H (red), and PAF-1-SO_3Ag (blue).

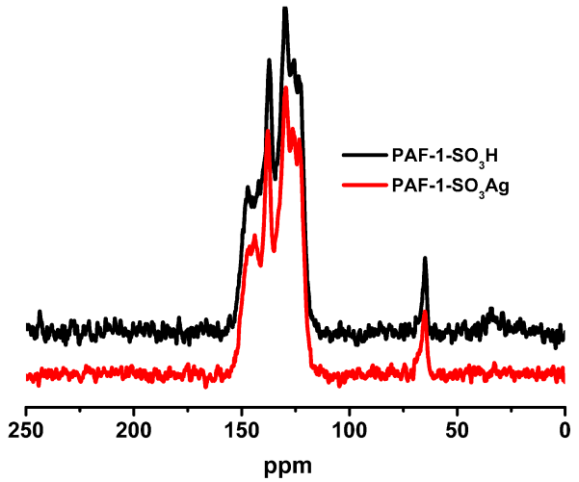

Figure S4. The ^{13}C NMR of PAF-1-SO_3H (black), and PAF-1-SO_3Ag (red).

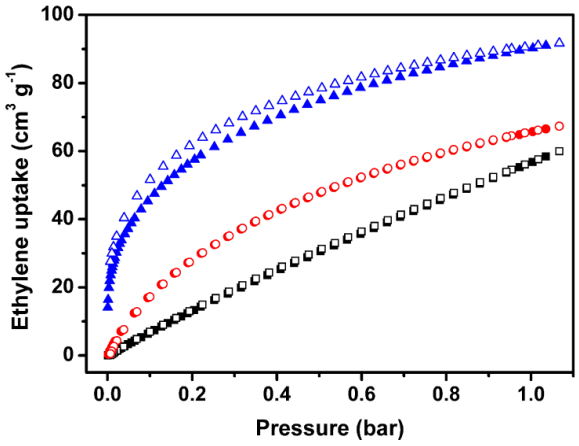

Figure S5. Comparison of ethylene sorption isotherms of PAF-1 (black), PAF-1-SO_3H (red), and PAF-1-SO_3Ag (blue) at 296 K.

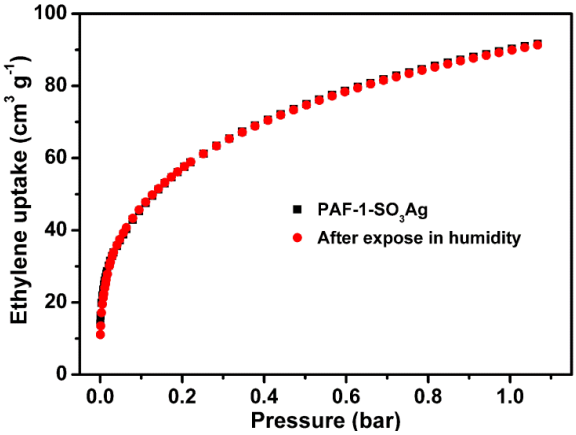

Figure S6. Comparison of ethylene adsorption isotherms of PAF-1-SO_3Ag and PAF-1-SO_3Ag after exposed in humidity (80%) for two days followed by activation at 105 °C.

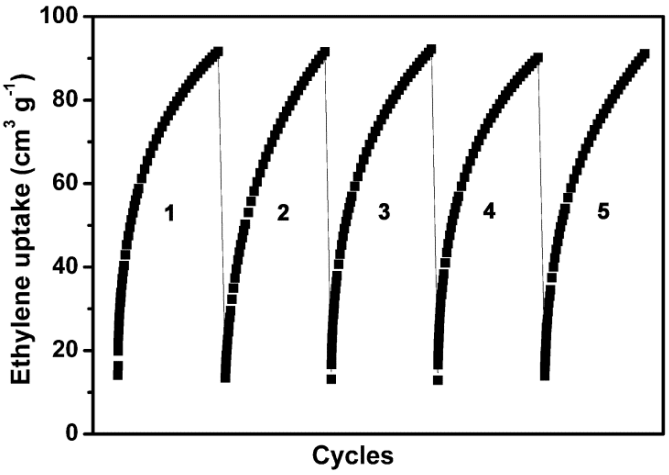

Figure S7. Five cycles of ethylene uptake for PAF-1-SO_3Ag at 296 K.

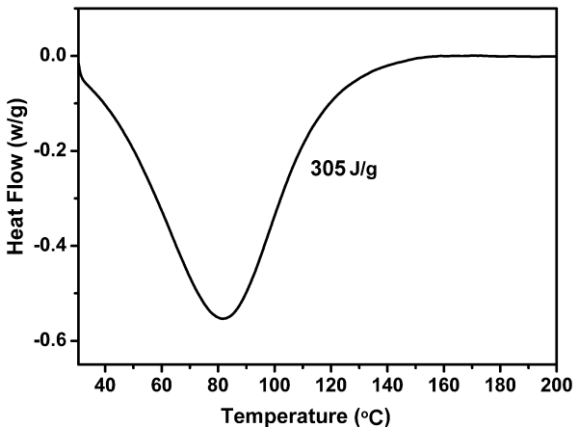

Figure S8. The DSC of ethylene desorption in PAF-1-SO_3Ag.

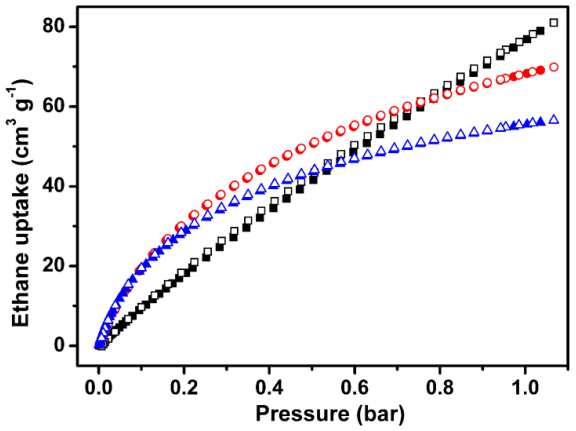

Figure S9. Comparison of ethane sorption isotherms of PAF-1 (black), PAF-1-SO_3H (red), and PAF-1-SO_3Ag (blue) at 296 K.

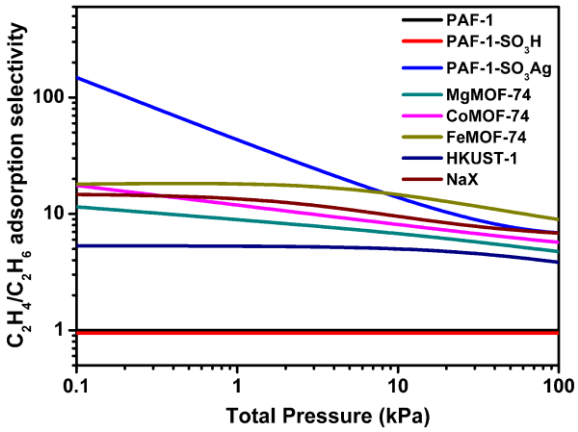

Figure S10. C_2H_4/C_2H_6 adsorption selectivities for PAF-1-SO_3Ag with PAF-1, PAF-1-SO_3 and other porous materials at 318 K. (Comments: The adsorption selectivities of PAF-1-SO_3Ag remain among the highest compared with other MOFs and NaX particularly in the low pressure range, further highlighting the important role of introducing strong π-complexation (Ag+ ion) into PAF for highly selective adsorption of ethylene over ethane. The slightly lower selectivity of PAF-1-SO_3Ag in the high pressure range compared to FeMOF-74 can be attributed to the relatively lower density of Ag(I) sites in PAF-1-SO_3Ag compared with the high density of Fe(II) sites in FeMOF-74. Nonetheless, PAF-1-SO_3Ag still outperforms all other MOFs and NaX in terms of adsorption selectivities for ethylene/ethane even at 318K).

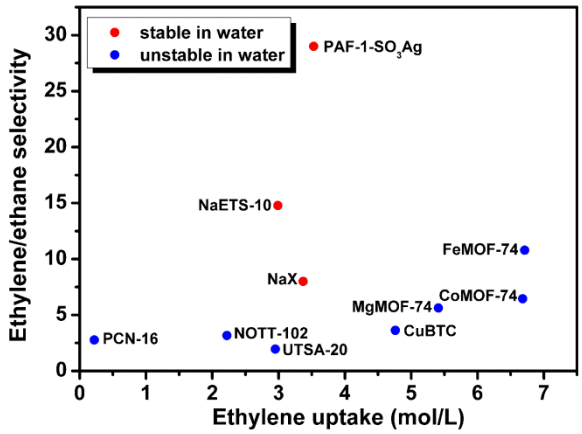

Figure S11. IAST calculations of the C_2H_4/C_2H_6 adsorption selectivity *versus.* the volumetric uptake capacity of ethylene for adsorption from an equimolar C_2H_4/C_2H_6 mixture at the total bulk gas phase at 296 K and 100 kPa. (Note: the volumetric uptake capacity of ethylene for PAF-1-SO_3Ag is estimated based upon its compressed pellet's density of 1.07 g/cm^3; whereas the volumetric uptake capacity of ethylene for others is estimated based upon their respective densities calculated from the crystal structures).

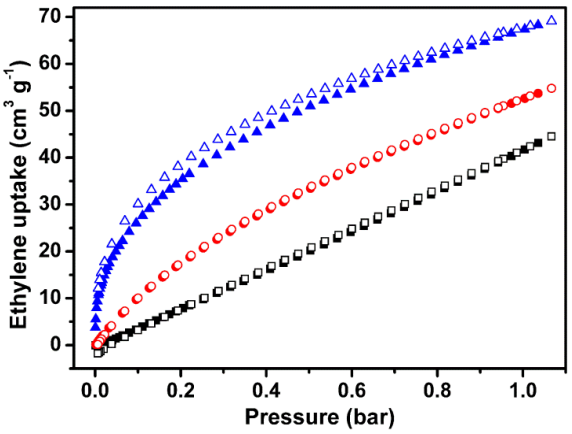

Figure S12. Comparison of ethylene sorption isotherms of PAF-1 (black), PAF-1-SO_3H (red), and PAF-1-SO_3Ag (blue) at 318 K.

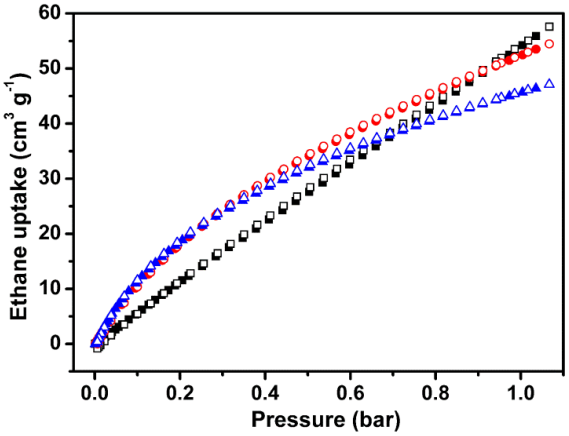

Figure S13. Comparison of ethane sorption isotherms of PAF-1 (black), PAF-1-SO_3H (red), and PAF-1-SO_3Ag (blue) at 318 K.

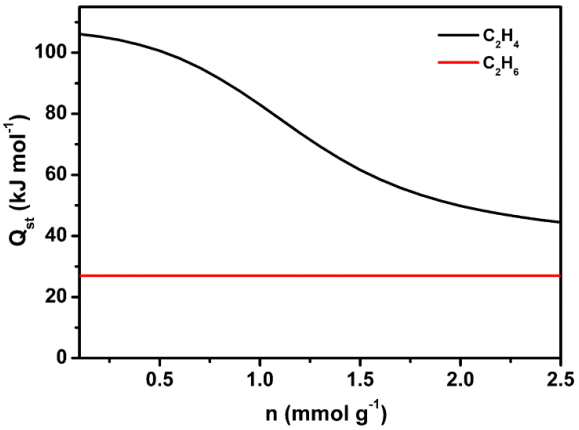

Figure S14. Comparison of isosteric heats of adsorption for ethylene (black) and ethane (red) in PAF-1-SO_3Ag.

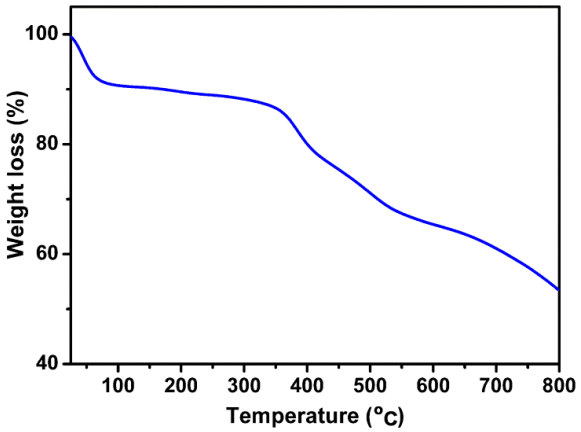

Figure S15. The TGA plot of PAF-1-SO_3Ag.

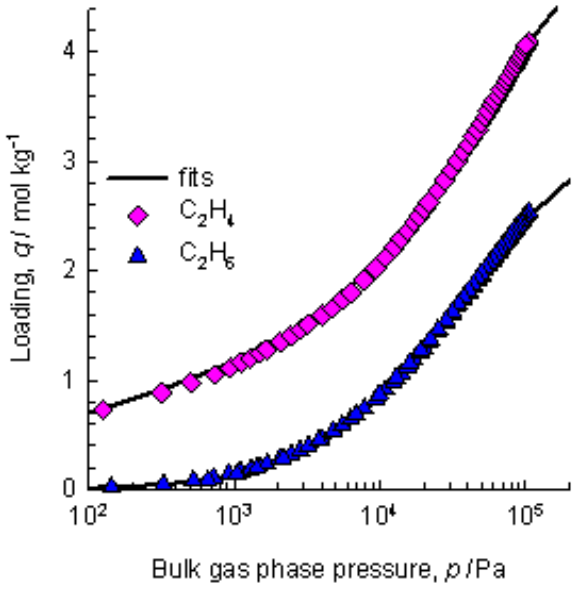

Figure S16. Comparison of the experimentally determined component loadings for C_2H_4 and C_2H_6 on PAF-1-SO_3Ag at 296 K with the isotherm fits using parameters specified in Table S1.

Table S1. Dual-Langmuir-Freundlich fits for C_2H_4 and C_2H_6 at 296 K in PAF-1-SO_3Ag.

	Site A			Site B		
	$q_{i,A,sat}$ mol/kg	$b_{i,A}$ $Pa^{-\nu_i}$	$\nu_{i,A}$ dimensionless	$q_{i,B,sat}$ mol/kg	$b_{i,B}$ $Pa^{-\nu_i}$	$\nu_{i,B}$ dimensionless
C_2H_4	3.6	5.86×10^{-5}	0.9	2	1.05×10^{-1}	0.35
C_2H_6	3.4	8.35×10^{-5}	0.9			

Table S2. Langmuir fits for C_2H_4 and C_2H_6 at 296 K in PAF-1.

	Site A		
	$q_{i,A,sat}$ mol/kg	$b_{i,A}$ $Pa^{-\nu_i}$	$\nu_{i,A}$ dimensionless
C_2H_4	15	2.04×10^{-6}	1
C_2H_6	15	2.91×10^{-6}	1

Table S3. Langmuir fits for C_2H_4 and C_2H_6 at 296 K in PAF-1-SO_3H.

	Site A		
	$q_{i,A,sat}$ mol/kg	$b_{i,A}$ $Pa^{-\nu_i}$	$\nu_{i,A}$ dimensionless
C_2H_4	4.5	1.87×10^{-5}	1
C_2H_6	4.5	2.12×10^{-5}	1

Table S4. *T*-dependent fits for 296 K and 318 K isotherm data

$$b_A = b_{A0}\exp\left(\frac{E_A}{RT}\right); \quad b_B = b_{B0}\exp\left(\frac{E_B}{RT}\right)$$

	Site A				Site B			
	$q_{A,sat}$ mol kg^{-1}	b_{A0} $Pa^{-\nu_i}$	E_A kJ mol^{-1}	ν_A dimensionless	$q_{B,sat}$ mol kg^{-1}	b_{B0} $Pa^{-\nu_i}$	E_B kJ mol^{-1}	ν_B dimensionless
C_2H_4	3.6	1.59×10^{-10}	30.6	0.94	1.8	2.25×10^{-10}	48	0.45
C_2H_6	3.1	6.51×10^{-10}	27	1				

Simulations of C_2H_4/C_2H_6 breakthroughs in packed beds

In order to demonstrate the feasibility of producing 99.95%+ pure C_2H_4 in a Pressure Swing Adsorption (PSA), we carried out breakthrough simulations for C_2H_4/C_2H_6 mixtures in a fixed bed of length L, packed with PAF-1-SO_3Ag that has a framework density $\rho = 1070$ kg/m^3; see schematic in Figure S17. The parameters that are used in the simulations are chosen on the basis of the experimental set-up and operating conditions. The length of the adsorber tube, L = 0.22 m. The voidage of the fixed bed was chosen $\varepsilon = 0.955$.

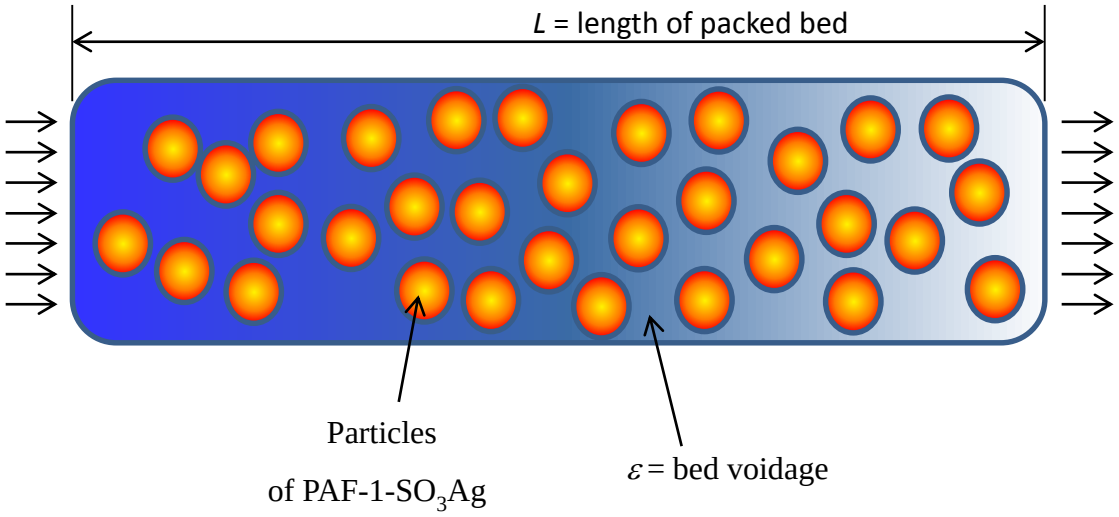

Figure S17. Schematic of a packed bed adsorber. The parameter values used in the simulations presented here are: L = 0.22 m; voidage of bed, ε = 0.955; interstitital gas velocity, v= 0.00085 m/s.

Assuming plug flow of the binary gas mixture through the fixed bed maintained under isothermal conditions at 296 K, the partial pressures in the gas phase at any position and instant of time are obtained by solving the following set of partial differential equations for each of the species i in the gas mixture.[1-7]

$$\frac{1}{RT}\frac{\partial p_i(t,z)}{\partial t} = -\frac{1}{RT}\frac{\partial\left(v(t,z)p_i(t,z)\right)}{\partial z} - \frac{(1-\varepsilon)}{\varepsilon}\rho\frac{\partial \bar{q}_i(t,z)}{\partial t}; \quad i = 1,2,...n \qquad (4)$$

In equation (4), t is the time, z is the distance along the adsorber, ρ is the framework density, ε is the bed voidage, v is the interstitial gas velocity, and $\bar{q}_i(t,z)$ is the *spatially averaged* molar loading within the crystallites of radius r_c, monitored at position z, and at time t. If the values of intra-crystalline diffusivities are large enough to ensure that intra-crystalline gradients are absent and the entire crystallite particle can be considered to be in thermodynamic equilibrium with the surrounding bulk gas phase at that time t, and position z of the adsorber

$$\bar{q}_i(t,z) = q_i(t,z) \qquad (5)$$

The molar loadings q_i are calculated on the basis of adsorption equilibrium with the bulk gas phase partial pressures p_i at that position z and time t. The adsorption equilibrium can be

calculated on the basis of the IAST. After discretization of the fixed bed into 100-200 slices, Equations (4) and Equation (5) need to be solved simultaneously using robust numerical procedures that are described in detail in the published literature.[11] The breakthrough simulation methodology has been rigorously tested and validated using a variety of experimental data on breakthroughs.[8]

Figure S18a compares the experimental data (ethane: dark green triangles; ethylene: blue triangles) with the breakthrough simulations (ethane: red circles; ethylene: black squares). We note reasonable agreement between the experiments and simulations. During the desorption cycle, it is possible to recover 99.95% pure C_2H_4 (Figure S19).

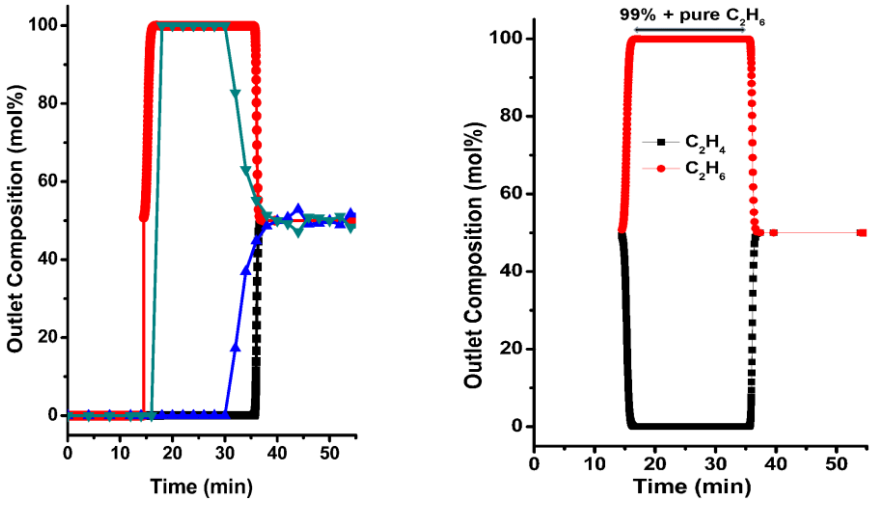

(a) (b)

Figure 18. (a) Simulated (ethane: red circles; ethylene: black squares) and experimental (ethane: dark green triangles; ethylene: blue triangles) breakthrough of an equimolar C_2H_4/C_2H_6 mixture in an adsorber bed packed with PAF-1-SO_3Ag in the adsorption phase of a PSA operation; (b) % C_2H_6 in the outlet gas of an adsorber bed packed with PAF-1-SO_3Ag in the adsorption cycle. (The inlet gas is maintained at partial pressures $p_1 = p_2 = 50$ kPa, at a temperature of 296 K).

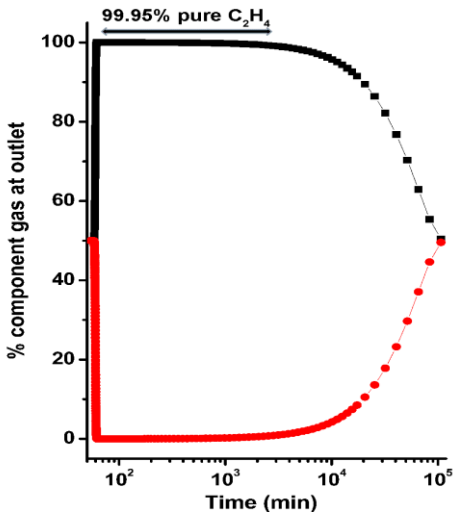

Figure S19. % C_2H_4 in the outlet gas of an adsorber bed packed with PAF-1-SO_3Ag in the desorption cycle. The contents of the bed, that is equilibrated at partial pressures $p_1 = p_2 = 50$ kPa, at a temperature of 296 K is purged by inert gas. For the calculations presented in the graph, the inert gas is not included in the calculation of the % compositions.

Notation

b_A dual-Langmuir-Freundlich constant for species *i* at adsorption site A, $Pa^{-\nu_i}$

b_B dual-Langmuir-Freundlich constant for species *i* at adsorption site B, $Pa^{-\nu_i}$

c_i molar concentration of species *i* in gas mixture, mol m^{-3}

c_{i0} molar concentration of species *i* in gas mixture at inlet to adsorber, mol m^{-3}

L length of packed bed adsorber, m

p_i partial pressure of species *i* in mixture, Pa

p_t total system pressure, Pa

q_i component molar loading of species *i*, mol kg^{-1}

$q_{sat,A}$ saturation loading of site A, mol kg^{-1}

$q_{sat,B}$ saturation loading of site B, mol kg^{-1}

$\bar{q}_i(t)$ *spatially averaged* component molar loading of species *i*, mol kg^{-1}

R gas constant, 8.314 J mol^{-1} K^{-1}

S_{ads} adsorption selectivity, dimensionless

t time, s

T absolute temperature, K

u superficial gas velocity in packed bed, m s^{-1}

v interstitial gas velocity in packed bed, m s^{-1}

V_p pore volume, m^3 kg^{-1}

z distance along the adsorber, and along membrane layer, m

Greek letters

ε voidage of packed bed, dimensionless

ν exponent in dual-Langmuir-Freundlich isotherm, dimensionless

ρ framework density, kg m^{-3}

τ time, dimensionless

Subscripts

i referring to component *i*

A referring to site A

B referring to site B

References

(1) Ruthven, D. M. Principles of Adsorption and Adsorption Processes; John Wiley: New York, 1984.

(2) Ruthven, D. M.; Farooq, S.; Knaebel, K. S. Pressure swing adsorption; VCH Publishers: New York, 1994.

(3) Yang, R. T. Gas separation by adsorption processes; Butterworth: Boston, 1987.

(4) Do, D. D. Adsorption analysis: Equilibria and kinetics; Imperial College Press: London, 1998.

(5) van den Broeke, L. J. P.; Krishna, R. *Chem. Eng. Sci.* **1995**, *50*, 2507.

(6) Walton, K. S.; LeVan, M. D. *Ind. Eng. Chem. Res.* **2003**, *42*, 6938.

(7) Krishna, R.; Baur, R. *Sep. Purif. Technol.* **2003**, *33*, 213.

(8) Krishna, R. *Microporous Mesoporous Mater.* **2014**, *185*, 30.

(9) Krishna, R.; Long, J. R. *J. Phys. Chem. C* **2011**, *115*, 12941.